Check for updates

View Article Online
View Journal

NJC

Accepted Manuscript

This article can be cited before page numbers have been issued, to do this please use: S. Mukhopadhyay, B. K. Kundu, P. Porwal, R. Kyarikwal and S. M. Mobin, *New J. Chem.*, 2019, DOI: 10.1039/C9NJ02342A.

This is an Accepted Manuscript, which has been through the Royal Society of Chemistry peer review process and has been accepted for publication.

Accepted Manuscripts are published online shortly after acceptance, before technical editing, formatting and proof reading. Using this free service, authors can make their results available to the community, in citable form, before we publish the edited article. We will replace this Accepted Manuscript with the edited and formatted Advance Article as soon as it is available.

You can find more information about Accepted Manuscripts in the author guidelines.

Please note that technical editing may introduce minor changes to the text and/or graphics, which may alter content. The journal's standard Terms & Conditions and the ethical guidelines, outlined in our author and reviewer resource centre, still apply. In no event shall the Royal Society of Chemistry be held responsible for any errors or omissions in this Accepted Manuscript or any consequences arising from the use of any information it contains.

View Article Online
DOI: 10.1039/C9NJ02342A

Mechanistic and thermodynamical aspects of pyrene based fluorescent probe to detect picric acid

Bidyut Kumar Kundu,[a] Pragti,[a] Reena,[a] Shaikh M. Mobin,[a] Suman Mukhopadhyay[a, b,]*

[a] Discipline of Chemistry, School of Basic Sciences, Indian Institute of Technology Indore, Simrol, Khandwa Road, Indore 453552, India

[b] Centre for Biosciences and Biomedical Engineering, School of Basic Sciences, Indian Institute of Technology Indore, Khandwa Road, Simrol, Indore 453552, India.

*E-mail: suman@iiti.ac.in; Fax: +91 731 2361; Tel: +91 731 2438 735

ABSTRACT

A remarkable PL based Schiff base probe [(2*E/Z*)-2-(9-**P**yrenylmethylene)hydrazide-2-**T**hiophene**C**arboxylic acid or PTC] has been employed for the rapid analytical detection of Cu^{2+} and picric acid (PA) up to nM level. Although, there are several literature reports on utilization of fluorescent probe for efficient explosives sensing in the last few years, however, there is no such report on the reaction spontaneity between 'probe-explosive' ensemble in equilibrium. Herewith, in this report for the first time, a detailed thermodynamic investigation has been included. Temperature dependent thermodynamic study reveals high negative Gibbs free energy as ΔG values of –120.3 to –123.0 kJ/mol have been obtained for PTC-PA adduct. Interestingly, there is a steady decrease of ΔG values with increase in temperature along with a consecutive increment in Stern-Volmer constant (K_{SV}). This suggests that the spontaneous adduct formation equilibrium for 'probe-picric acid' ensemble becomes stronger with rise in temperature. A negative ΔH value of -81.77 kJ/ mol confirms that the spontaneous adduct formation in equilibrium is exothermic in nature. Apart from picric acid sensing, PTC and PTC + Cu^{2+} complex possesses cell permeable ability, and thus, they have been explored for the living cell imaging. Moreover, theoretical and experimental agreement on the PET based sensing mechanism correlates that the extensive conjugation of pyrene system attached to the adjacent imine along with the higher electric potential encompassing thiophene ring are very much instrumental for PTC to act as PA sensor.

INTRODUCTION

In last few years, enormous focus has been given to detect and quantify various chemical entities in environment and biological systems. Developing new probes for efficient and cost effective methodology for sensing a particular entity has taken the forefront of chemical research. Though, massive number of molecular probes have been introduced for sensing different molecules or groups, the mechanistic and thermodynamical aspects of sensing

Published on 10 June 2019. Downloaded by Nottingham Trent University on 6/22/2019 1:21:58 PM.

New Journal of Chemistry Accepted Manuscript

View Article Online
DOI: 10.1039/C9NJ02342A

Published on 10 June 2019. Downloaded by Nottingham Trent University on 6/22/2019 1:21:58 PM.

largely remains in backseat. One of such area is the detection of common explosives which are based on nitro-aromatic compounds (NACs), such as trinitrophenol/ picric acid (TNP/ PA), trinitrotoluene (TNT). The importance of the detection of such molecules like TNT and cyclotrimethylenetrinitramine (RDX) lies in the fact that they are the potential chemicals which are quite capable to explode and bring out considerable damages in terms of life and property if utilized with evil intentions.[1] On the other hand PA with easily dissociable phenolic proton has been found to be more corrosive than that of RDX and TNT.[2-6] Having incredible water solubility, PA is responsible for several diseases or symptoms associated to groundwater poisoning, *viz* anaemia, nausea, vomiting, asphyxiation, sycosis, skin/ eye itching, abdominal pain, and liver or kidney damage.[3, 7] Furthermore, picric acid is widely used in fireworks, pharmaceuticals, rocket fuels, leather and dye industries but also it has been accepted as an environmental pollutant and is quite dangerous to humans and wildlife.[8-10] The acceptable tolerance concentration of picric acid in groundwater is 0.001 mg/L.[11] Thus, the trace detection of PA has an unmet need to reduce environmental pollution as well.

Though, there are numerous analytical techniques to detect NACs, but the most widely used methodology is the utilization of fluorescent probes.[12, 13] There are already several reports where change in fluorescent pattern has been introduced to detect NACs.[14, 15] However, to the best of our knowledge, there is no report where the thermodynamical aspects, which is a key to understand the mechanistic pathways have been explored for detection of PA. Among the different kinds of probes quantum dots, nanoparticles, COFs/ MOFs, oligomers, or conjugated polymers, micro or nano aggregates, *etc.* found to be common.[8, 16-20] Various mechanistic approaches (such as PET, ESIPT, FRET, RET, chemodosimeters, AIE *etc*.) have been proposed to explain the probable cause behind FL quenching during explosive sensing.[2, 19, 21, 22] Among them donor-acceptor theory is the most common explanation, which involves the charge or energy transfer from the sensor's photoexcited state to the ground state of NACs.[23]

To investigate the mechanistic and thermodynamical aspects of sensing of NACs, herein, we have designed and developed a pyrene based small molecule chemosensor, PTC (where, PTC = (2*E/Z*)-2-(9-**P**yrenylmethylene)hydrazide-2-**T**hiophene**C**arboxylic acid) (Scheme 1) for the efficient detection of PA which has been found to be effective with a limit of detection (LOD) value of 19 nM in acetonitrile (ACN) *via* FL spectroscopy. LOD value in nM range suggest that PTC can act as ultrasensitive fluorescent sensor for PA. The pyrene as well as thiophene based system has been selected because of (a) π-electron rich, planar, aromatic

New Journal of Chemistry Accepted Manuscript

View Article Online
DOI: 10.1039/C9NJ02342A

Published on 19 June 2019. Downloaded by Nottingham Trent University on 6/22/2019 1:21:58 PM.

conjugated nature, which enables the 1D π-π stacking to support the exciton migration, (b) H-bonding, π-π stacking and van der Waal forces based supramolecular interactions which helps the chemosensor to form the stronger self-assembly,[24] and (c) thiophene accelerates electron transfer to NACs due to its higher electric potential.[25-27] Although PTC possesses considerable FL emission, however, a low concentration of PA solution can be sufficient to quench it. Furthermore, selective addition of copper ion (Cu^{2+}) can enhance the FL intensity of PTC by ten folds because of PTC-Cu^{2+} complex formation. In turn, this Cu^{2+} complex can also act as a fluorescent probe towards PA. The fluorescence of PTC and its Cu^{2+} complex can be easily visible in naked eyes under UV chamber. Detailed reaction spontaneity for PTC-PA adduct was fully illustrated by temperature variable thermodynamical study, and corresponding ΔH, ΔS, and ΔG parameters have been determined.

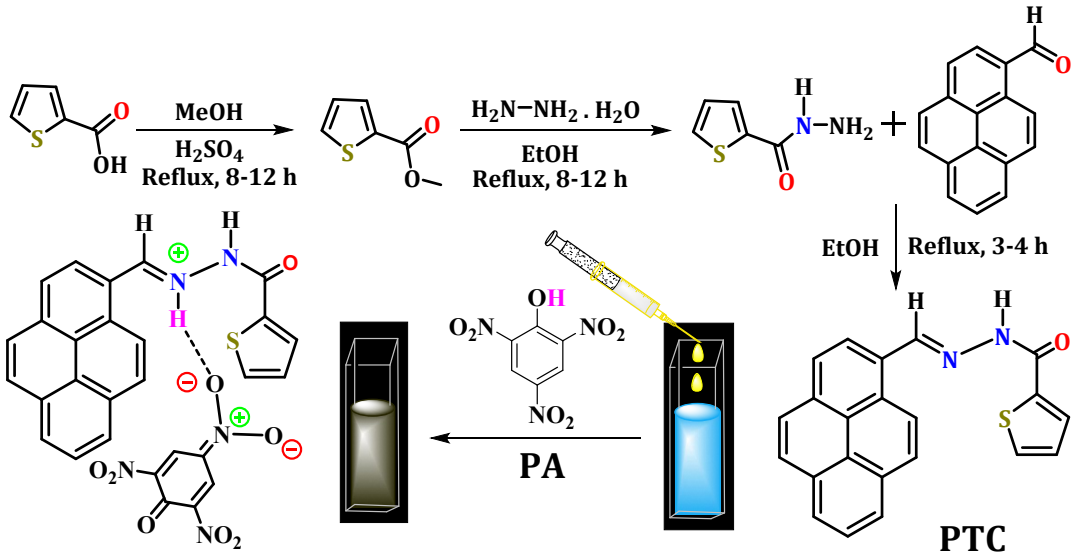

Scheme 1. Synthesis of PTC and corresponding sensing representation with PA.

Several reports of Schiff base probes as PA sensor have been reported in the past few years but mechanistic pathways are unknown for many of such cases. In this circumstances, we have investigated the probable mechanistic pathway by correlating the experimental overviews with that of theoretical calculations. The corresponding DFT and TDDFT calculations has been carried out by Gaussian 09 software using B3LYP (6-31G) and CAMB3LYP basis sets respectively.

EXPERIMENTAL SECTION

General Remarks

New Journal of Chemistry Accepted Manuscript

View Article Online
DOI: 10.1039/C9NJ02342A

Published on 10 June 2019. Downloaded by Nottingham Trent University on 6/22/2019 1:21:58 PM.

The analytical grade solvents and reagents were acquired from Aldrich, Merck, and TCI and used without purification. Thiophene-2-carboxylic hydrazide was prepared according to the previous report.[28] Please check ESI† for all the characterization data of PTC, *viz*. Fig. S1-S3†.

Instrumentation

Kindly consult ESI† for detailed instrument specifications.

Synthesis of PTC [(2*E/Z*)-2-(9-Pyrenylmethylene)hydrazide-2-ThiopheneCarboxylic acid)]

Thiophene carboxylic acid was first refluxed in methanol for 8-12 h to get the corresponding ester. Now, hydrazine hydrate was added and refluxed further for 8-12 h. to produce the white residue of thiophene-2-carboxylic hydrazide.

The solution of thiophene-2-carboxylic hydrazide (2 mmol = 284 mg) in MeOH (10 mL) was added to a methanolic solution (30 mL) of pyrene-1-carboxaldehyde (2 mmol = 460 mg). The mixture was then refluxed for 8 h at 70 ^{o}C followed by the filtration ad washed through MeOH and diethylether. The solid crystalline residue was dried over vacuum and collected for further characterization. X-ray diffraction suitable deep yellow colored single crystals were obtained after 9 days by slow evaporation in DMF solvent at room temperature.

Yield: 92% (orange solid), M.p. 265-268 ^{o}C. ^{1}H NMR (400.13 MHz, 298K, D_6-DMSO, δ ppm, E:Z = 1.4:1) : δ (E-isomer) = 7.29 (1H, t, Py-H), 7.99 (1H, d, Th-CH), 8.14 (2H, d, Py-H), 8.28 (2H, d, Py-H), 8.37 (4H, d, Py-H), 8.56 (1H, t, Th-CH), 8.83 (1H, d, Th-CH), 9.48 (1H, s, Py-CH=N), 12.07 (1H, s, exchangeable C=O-NH) ppm; (Z-isomer) = 7.27 (1H, t, Th-Py-H), 7.92 (1H, d, Th-CH), 8.10 (2H, d, Py-H), 8.21 (2H, d, Py-H), 8.36 (4H, d, Py-H), 8.55 (1H, t, Th-CH), 8.73 (1H, d, Th-CH), 9.27 (1H, s, Py-CH=N), 11.96 (1H, s, exchangeable C=O-NH) ppm (Fig. S1a); ^{13}C NMR (100.61 MHz, 298 K, D_6-DMSO, δ ppm): (E/Z-isomer) = δ 124, 126, 127, 128, 129, 130, 131, 132, 135, 142, 146, 158, 161 (Fig. S1b). FT-IR (KBr, cm^{-1}): 3220 and 3063 (N-H), 1635 (C=O), 1560 (C=N) (Fig. S2). Anal. Calcd (%) for $C_{22}H_{14}N_2OS$: C, 74.55; H, 3.98; N, 7.90; O, 4.51; S, 9.05. Found: C, 74.29; H, 3.57; N, 7.94; S, 8.93 %. HRMS in HPLC MeOH (+, m/z): $(C_{22}H_{14}N_2OS + Na)^+$: 377.0719 (100%) (Fig. S3).

Preparation of stock for photo-physical studies

New Journal of Chemistry Accepted Manuscript

View Article Online
DOI: 10.1039/C9NJ02342A

Published on 19 June 2019. Downloaded by Nottingham Trent University on 6/22/2019 1:21:58 PM.

Please see the supporting information (Section S3†) for more details. In addition, Section S5† describes the crystallographic information about PTC probe.

RESULTS AND DISCUSSION

Synthesis and characterization of PTC

PTC was isolated as yellow solid by Schiff base condensation and further dark yellowish single crystals were grown in DMF medium in 9 days (see ESI† for details). Chemosensor was well characterized by NMR (Fig. S1), FTIR (Fig. S2), HRMS (Fig. S3) and single crystal X-ray crystallography (Fig. 1a). ^{1}H NMR data suggest that PTC is in E/Z isomeric form and the corresponding ratio is 1.4:1. Prominent IR stretching modes are observed at 3220 and 3063 cm^{-1} (N-H), 1635 cm^{-1} (C=O), 1560 cm^{-1} (C=N).[29, 30] HRMS in HPLC MeOH having chemical formula $(C_{22}H_{14}N_2OS + Na)^+$ has been observed at 377.0719. Structural elucidation of PTC indicates a monoclinic crystal system with P 21/c space group. The corresponding bond lengths and bond angles are summarized in Table S1-2. Several supramolecular non-covalent interactions such as H-bonding, π-π stacking, CH-π interaction *etc*. contribute together to form a dimeric (Fig. S4a) and 1D/ 2D polymeric frameworks (Fig. 1b-c and Fig. S4b-d).

Photo-physical studies

Solubility in numerous solvents help the chemosensor PTC to avail absorption or emission spectroscopy as a sensing tool in a broader way (Fig. S5). Various wavelength maxima of PTC in different solvents are summarized in Table S3 along with log ε values. This solvatochromic behavior reveals that absorption spectra at ~370 nm in organic solvents are having larger log ε values in comparison to those in 100% aqueous medium. This may be due to the easy formation of intermolecular hydrogen bonds between PTC and H_2O in fully aqueous or buffer medium. Although, no such considerable change was observed in the position of λ_{max}/ λ_{ex}. The metal ions sensing response of PTC was explored *via* UV-Vis and FL experiments (Fig. S6). It shows that Cu^{2+} ion can be selectively sensed among all essential metals, which can be visualized even in naked eye under UV light through paper strip experiment (Fig. S7). Sensor shows the absorption maximum at 274, 368, and 400 nm which are assignable as the intra-ligand π-π* and n-π* transitions. Two isosbestic points generated at 352 and 384 nm along with a new peak at 436 nm (LMCT) upon complexation with Cu^{2+} (Fig. S8).

New Journal of Chemistry Accepted Manuscript

View Article Online
DOI: 10.1039/C9NJ02342A

Published on 10 June 2019. Downloaded by Nottingham Trent University on 6/22/2019 1:21:58 PM.

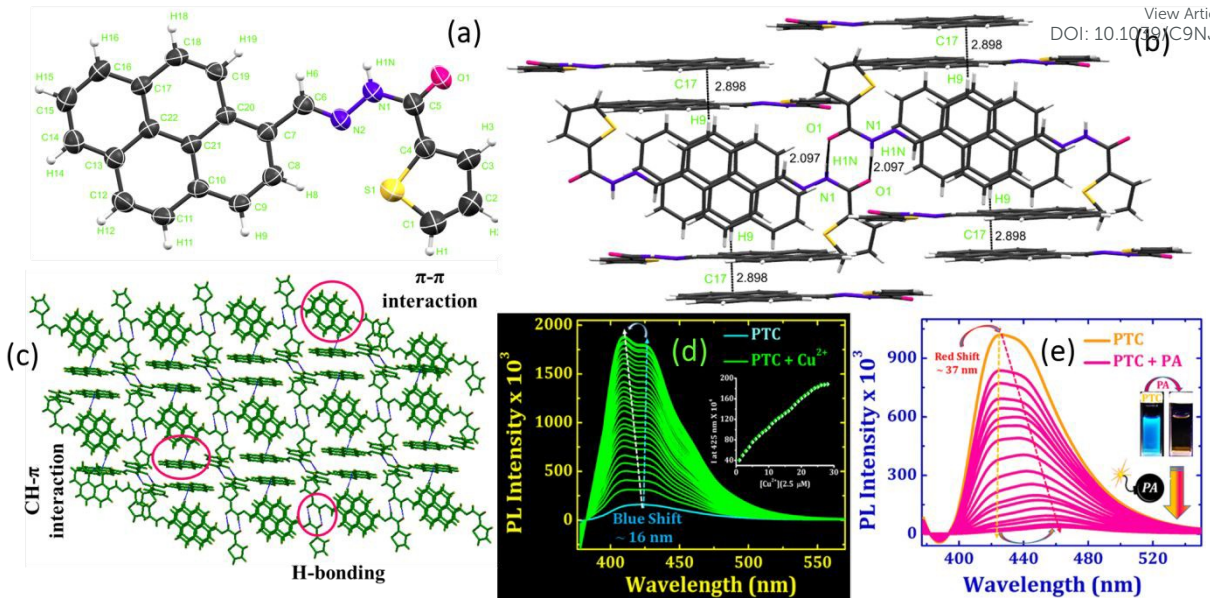

Fig. 1. (a) Single crystal x-ray diffracted structure of sensor PTC, (b) and (c) Several supramolecular interactions (intermolecular hydrogen bonding, CH-π, and π-π interactions) to form self-assembled 2D framework, (d) fluorescence titration of PTC by Cu^{2+} ion, and (e) titration profile of PTC (0.8 μM in acetonitrile, slit: 2) in presence of PA (10-100 nM; $\lambda_{excitation}$: 368 nm, and $\lambda_{emission}$: 425 nm).

Quantum yield (Φ) calculation

The fluorescence quantum yield (Φ) was calculated as per following equation:[31]

$$\Phi_s = \frac{Abs_R}{Abs_S} \times \frac{Area_S}{Area_R} \times \frac{\eta_S}{\eta_R} \times \Phi_R$$

Where 'Φ' denotes the fluorescence QY, 'Abs' denotes optical density, 'Area' terms denote the integration under the fluorescence curve, and the refractive index as 'η' (η = 1.3284 for MeOH solvent medium). Subscripts 'R' and 'S' stand for the respective parameters belonging to the experimental reference as well as the sample.

Φ of PTC (0.007) increases more than 10 folds upon addition of Cu^{2+} (Φ = 0.076) with respect to Cumarin (ϕ_R = 0.09 in MeOH). However, increasing concentration of PTC (10-307 nM) shows a good FL response (Fig. S9). Moreover, with increasing concentration of Cu^{2+} ion emission intensity increases with a blue shift of ~16 nm (shift from 425 to 409 nm) (Fig. 1d and Fig. S10a).

Binding studies of PTC towards Cu^{2+} and PA

New Journal of Chemistry Accepted Manuscript

View Article Online
DOI: 10.1039/C9NJ02342A

Published on 19 June 2019. Downloaded by Nottingham Trent University on 6/22/2019 1:21:58 PM.

Fig. S10b represents the B-H plot of PTC-Cu^{2+} adduct. From which association constant value was found to be 1.37×10^4 M^{-1}. Moreover, the detection limit (LOD) of PTC towards Cu^{2+} has been evaluated as 3.5×10^{-7} M (Fig. S10c). Apart from that, PTC possesses superior activity up to nanomolar range to selectively detect PA among other NACs. Although, most of the recent literatures are focused to detect PA from various nitro explosives, but unfortunately specific sensing of PA among other similar substituted nitro phenols (NPs) are uncommon. Herewith, we focus to find out (a) the exclusive binding motif of PTC towards PA and / or (b) the importance of –OH group for the detection of PA with respect to rest of the NPs. Fig. S11 shows the optical density (O.D) values of PTC in presence of different NACs. Notably, no such change in O.D values were observed in the λ_{max} range of PTC except PA, which shows considerably high molar extinction coefficient in compared to PTC. The detailed photophysical properties of PA sensing by PTC were investigated in ACN medium at room temperature. Firstly, the large blue shift of 24 nm (from 368 to 344 nm) was observed in UV-Vis titration with PA. Consequently, λ_{max} at 274 nm of PTC disappears upon gradual addition of PTC and generates a new peak at 237 nm (Fig. S12). Furthermore, a bathochromic shift of 37 nm was observed when PTC was titrated with PA (from 425 to 462 nm) (Fig. 1e).

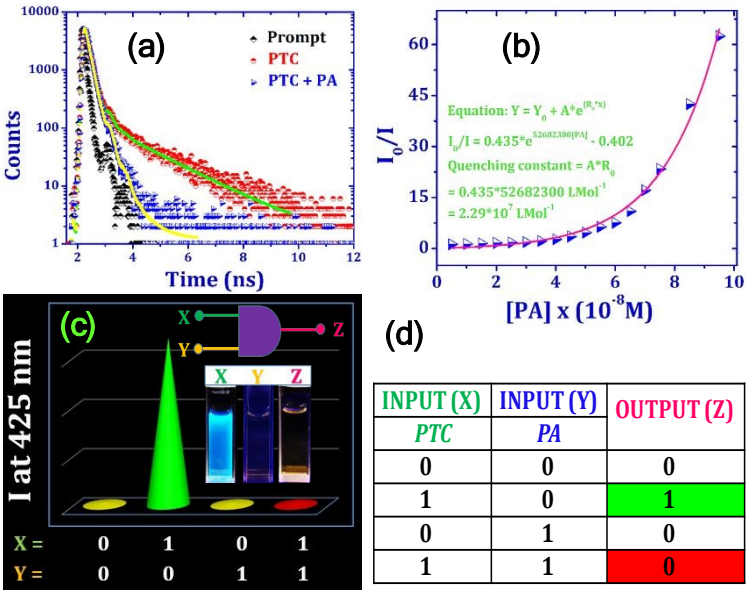

INPUT (X) PTC	INPUT (Y) PA	OUTPUT (Z)
0	0	0
1	0	1
0	1	0
1	1	0

Fig. 2. (a) Lifetime decay diagram of PTC and PTC-PA (λ_{ex} at 368 nm, and $\lambda_{collection}$ at 425 nm, concentration: 1.0 μM). (b) Nonlinear Stern-Volmer (K_{SV}) plot of PTC in presence of quencher, PA. (c) INHIBIT gate for Logic responses (Inset); where X and Y are inputs and Z is the output signal(s) having respective visual identification. (d) Truth table representation using PTC and PA as inputs, and the current signals of the logic gate at 425 nm emission.

New Journal of Chemistry Accepted Manuscript

View Article Online
DOI: 10.1039/C9NJ02342A

Published on 10 June 2019. Downloaded by Nottingham Trent University on 6/22/2019 1:21:58 PM.

Fluorescence response of PA was drastically changed upon introduction of various NACs and were summarized in Fig. S13a. Colorimetric histogram of PTC (Fig. S13b) can distinguish PA among other NACs, which can be also visualized in naked eye under UV chamber. Excited-state lifetimes of probe and sensor adduct(s) have been calculated according to the following equations:[31, 32]

$$F(t) = \sum_{i=1}^{2} a_i \exp\left(-\frac{t}{\tau_i}\right)$$

The above equation has been used for the determination of time-resolved emission decays, where, F(t) is the FL decay at normalized condition, α_i is the pre-exponential factor, and a_1 and a_2 denotes the normalized amplitude having decay component τ_1 and τ_2 respectively. The equation below gives the value of average lifetime (in ns):

$$\langle \tau \rangle = \sum_{i=1}^{2} a_i \tau_i$$

where, a_i is the contribution of the ith decay component, and $a_i = \alpha_i/\Sigma\alpha_i$.

Lifetime decay dynamics of PTC and PTC-PA are shown in Fig. 2a and the corresponding parameters are summarized in Table S4. PTC shows three exponential fitting with small contribution from faster (< 1 nS) nonradiative decays. Upon treatment of PTC with Cu^{2+}, the lifetime considerably increases to restrict the nonradiative decay, therefore enhancing emission intensity. However, addition of PA shows a huge contribution from faster nonradiative decay (0.074 nS).

The host-guest PTC-PA ensemble exhibits association constant of 6.814×10^6 M^{-1} (by using B-H plot: K_a = intercept : slope ratio, when plotted (A_0/A_0-A) vs 1/[PA] following linear equation, where A_0 is the O.D. value in absence of PA), which further fitted with online 'BindFit v0.5- Supramolecular' server (Fig. S14a-b).[31] As displayed in Fig. 2b, the Stern-Volmer (S-V) quenching constant (K_{SV}) was calculated by S-V equation:[33] $I_0/I = 1 + K_{SV}[PA]$, where I_0 and I are the fluorescence intensities of PTC before and after the addition of PA, and [PA] is the molar concentration of PA during fluorescence titration at 425 nm. Two distinct regions in S-V plots (Fig. 2b and Fig. S15a) suggest: (a) static quenching in the lower concentration of PA, and (b) H-bonding energy transfer process or self-absorbance of PA to facilitate the dynamic quenching in the higher range of [PA].[3] Moreover, this higher

New Journal of Chemistry Accepted Manuscript

View Article Online
DOI: 10.1039/C9NJ02342A

Published on 10 June 2019. Downloaded by Nottingham Trent University on 6/22/2019 1:21:58 PM.

linear concentrations range of S-V plot provides a signature of ultrasensitive detection ability of PTC towards PA. K_{SV} was estimated as 2.29×10^7 M^{-1} having an excellent detection limit of 19 nM (Fig. S15b) and the high K_{SV} value make PTC a potential candidate to act as a sensor with respect to other reported molecular probes. Furthermore, fluorescence "off-on" switching of PTC and PTC + Cu^{2+} with PA encouraged us to explore the field of molecular switches and logic gates. As described in Fig. 2c, green output signal was only observed when X = 1 and Y = 0, where, X is the input for PTC or PTC + Cu^{2+} and Y defined the same for PA. Output, Z behaves like an INHIBIT logic gate (Fig. 2d),[34] when both the inputs are its "on" state (= 1). Interestingly liquid phase FL response was further employed for the naked eye visualization of PA through paper strip method.

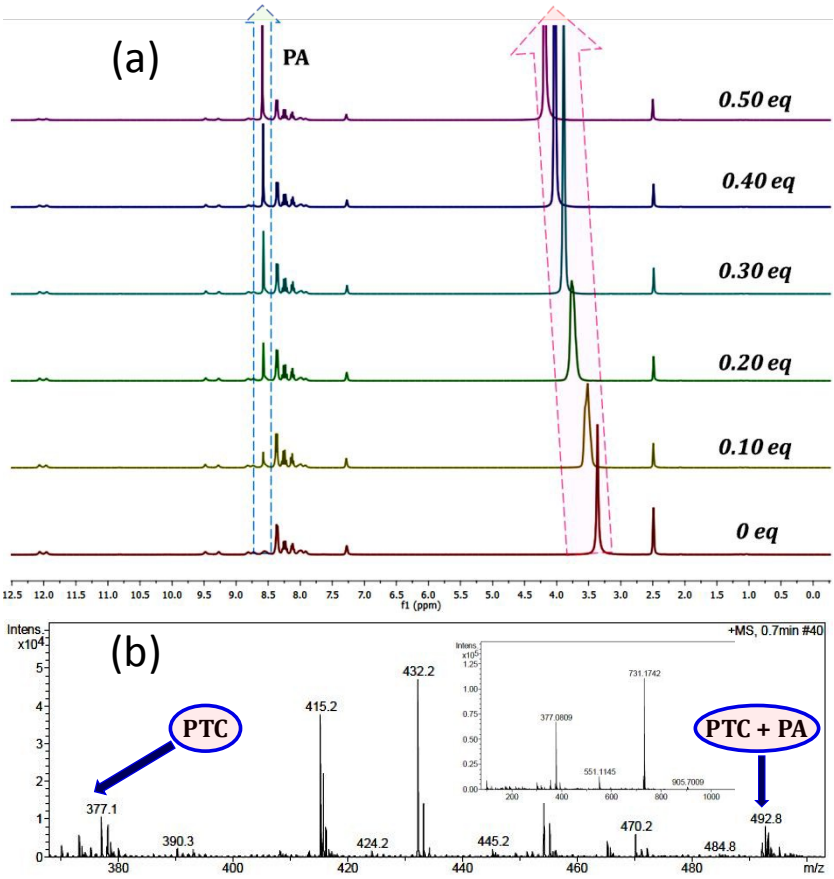

Fig. 3. Binding affinity studies through: (a) sequential ^{1}H NMR titration of PTC and PA (400.13 MHz, D_6-DMSO, 0.5 mL, δ in ppm) at room temperature, (b) ESI-MS spectra in CH_3CN solvent representing the formation of intermediate 'PTC-PA'; Inset: same for the chemosensor PTC in absence of PA.

^{1}H NMR titration and ESI-MS were employed to have an insight into the binding affinity of PTC with Cu^{2+} or PA. As shown in Fig. S16, the slight peak shifting as well as decrement in

New Journal of Chemistry Accepted Manuscript

View Article Online
DOI: 10.1039/C9NJ02342A

Published on 10 June 2019. Downloaded by Nottingham Trent University on 6/22/2019 1:21:58 PM.

peak intensities in the aromatic zone (δ ~ 8.4 ppm) indicates the favoured metalation course. Furthermore, a consecutive peak broadening occurs upon increase in the equivalent ratio of Cu^{2+} ion in the aliphatic zone (δ ~ 3.3 ppm), which might be responsible for the interaction with water. Apart from that, the interaction between PTC and PA are depicted in Fig. 3a and Fig. S17. All the ^{1}H NMR titration were conducted at room temperature in DMSO-d_6 medium. The proton signal at δ ~ 12.07 ppm surprisingly vanishes upon gradual increase in the concentration of PA. This might be attributed to the formation of hydrogen bonds between -NH proton of PTC and PA. A slight up field shift belongs to pyrene ring protons at δ ~ 7.29 ppm was observed under similar condition. A new singlet peak at δ ~ 8.78 ppm appears during the course of titration, which is associated with the aromatic protons of PA. So, we may conclude that the formation of strong intermolecular H-bonds between sensor and PA initiates the effective fluorescence quenching process. Furthermore, ESI mass spectral analysis shows the peaks at 417.0 and 492.8 (Fig. S18 and Fig. 3b) for 1:1 binding of PTC with Cu^{2+} and PA, which is also corroborated with the theoretical calculations. In addition, the 1:1 stoichiometric coefficient was confirmed by Jobs plot measurement having mole fraction 0.5 with respect to the sensor (Fig. 4a) for detection of PA. An abrupt FL quenching of chemosensor PTC has been observed within a few seconds upon interference of PA as shown in Fig. 4b. There was no further change in fluorescence intensity has been observed upon standing.

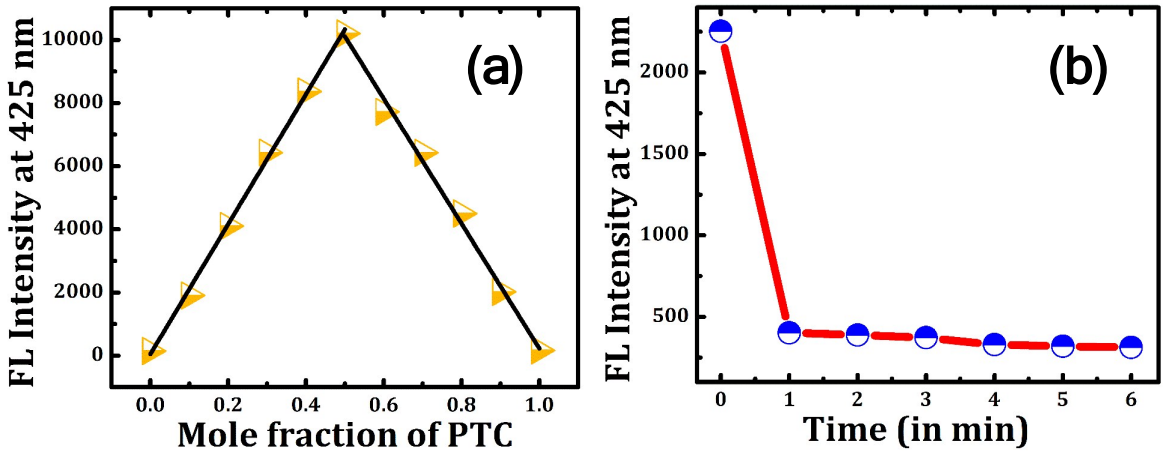

Fig. 4. (a) Jobs plot to better understand the stoichiometric coefficient during binding experiment between PTC and PA. (b) Time dependent FL intensity during the course of PTC titration with PA in acetonitrile solution.

Thermodynamical aspects

New Journal of Chemistry Accepted Manuscript

View Article Online
DOI: 10.1039/C9NJ02342A

Published on 19 June 2019. Downloaded by Nottingham Trent University on 6/22/2019 1:21:58 PM.

Thermodynamic parameters such as ΔH, ΔS, and ΔG have been evaluated using van't Hoff equation: [$\ln K_b$ = (ΔS/ R) - (ΔH/ RT)], and Gibbs free energy equation: ΔG = ΔH - TΔS, where K_b, R, ΔH, ΔS, and ΔG defines binding constant, real gas constant, enthalpy change, entropy change, and standard Gibbs free energy change (Fig. 5). It gives an overview about extent of PTC-PA adduct formation in equilibrium and the corresponding thermodynamic parameters have been summarized in Table S5. As depicted in Fig. 6A, the high negative value of ΔG (–120.3 to –123.0 kJ/ mol) suggests the favoured the adduct formation. A negative ΔH value of -81.77 kJ/ mol has been found for the similar reaction profile, confirming that the adduct formation is exothermic in nature. Fig. 6B depicts the decreasing trend of the intensity of dark spots by decreasing the concentration of PA (10 to 0.0001 μM) in a fixed concentration of PTC immersed test paper. The spot detection technique for PA can be also utilized for the solid phase detection (Fig. S19).

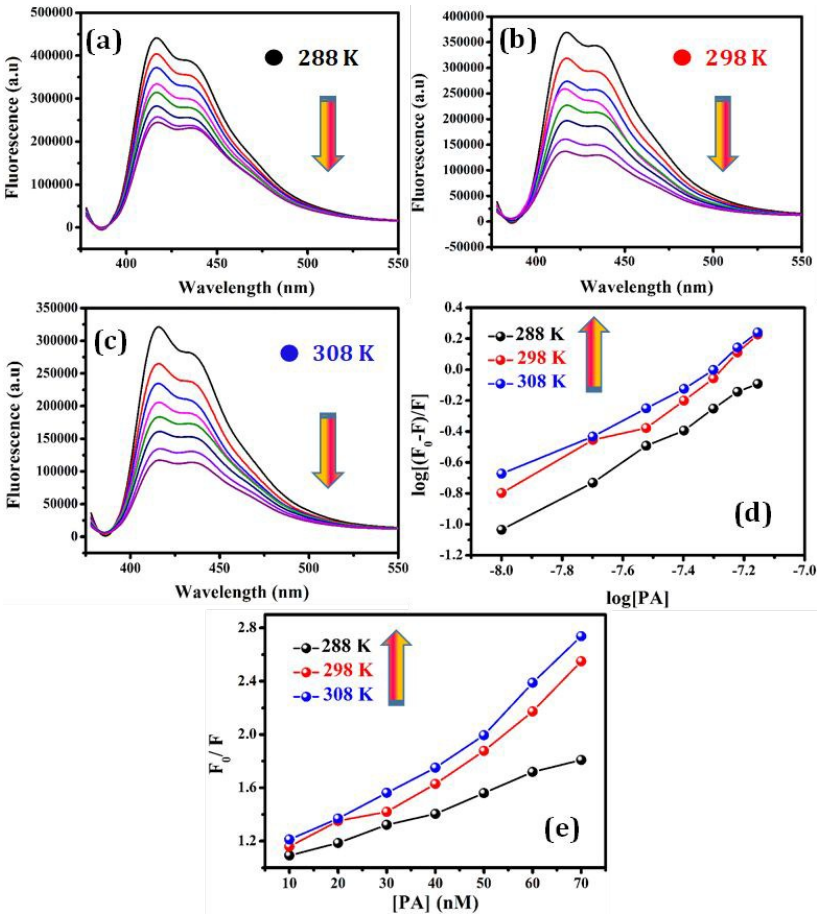

Fig. 5. (a-c) Temperature dependent fluorescence quenching of PTC in presence of picric acid (solvent: acetone, temperature range: 288-308 K, [PTC] = 0.5 μM, [PA] = 10-70 nM). (d) Scatchard plots of the PTC–PA ensemble. (e) Steady-state Stern–Volmer plots of PTC at three different temperatures (288 K, 298 K, and 308 K) as a function of PA concentrations.

New Journal of Chemistry Accepted Manuscript

View Article Online
DOI: 10.1039/C9NJ02342A

Published on 10 June 2019. Downloaded by Nottingham Trent University on 6/22/2019 1:21:58 PM.

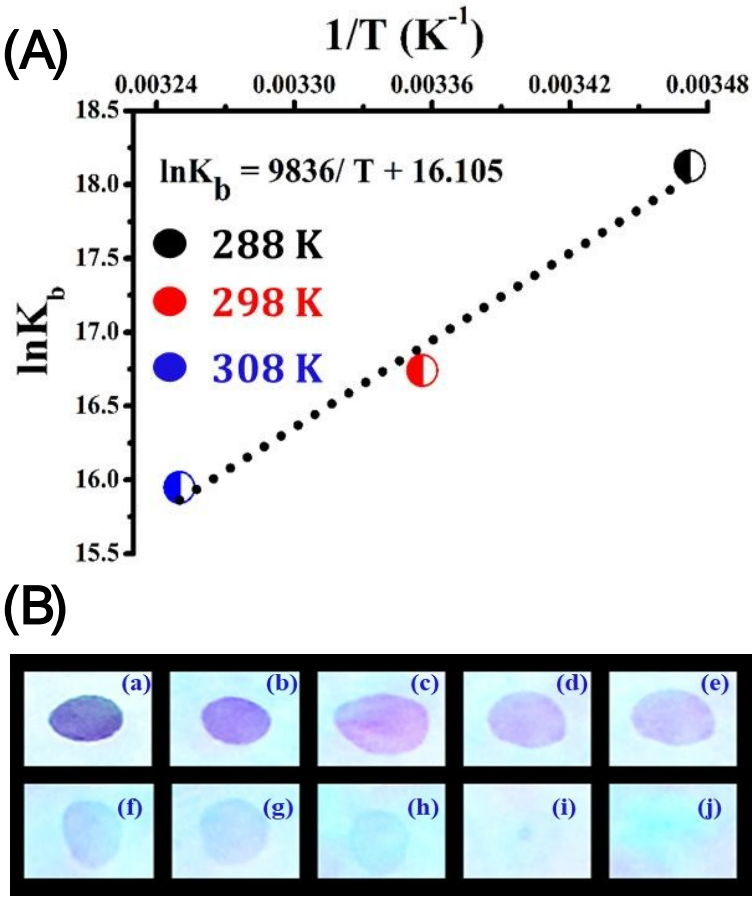

Fig. 6. (A) van't Hoff plot for PTC-PA adduct (solvent: acetone, temperature range: 288-308 K). (B) PTC immersed 'paper strip experiment' on the basis of different concentration ratio of PTC : PA; where [PA in μM] are (a) 10 μM, (b) 1.0 μM, (c) 0.1 μM, (d) 0.01 μM, (e) 0.008 μM, (f) 0.004 μM, (g) 0.001 μM, (h) 0.0005 μM, (i) 0.0001 μM, (j) 0 μM.

Theoretical calculations

Despite of several experimental evidences, it is worthy to investigate it further by theoretical approach. For better understanding, the correlation between the experimental and theoretical agreement of sensing mechanism as well as optical responses has been established by density functional theory (DFT) and time-dependent density functional theory (TDDFT) calculations.

Probable sensing mechanism

The introduction of donor-acceptor e^- transfer theory can explain the FL quenching phenomenon. The electron densities of HOMO (-5.33 eV) of PTC are delocalized only on pyrene moiety (donor part), not on the thiophene ring (acceptor part), however e^- density spread over both the pyrene and thiophene in case of LUMO (-2.12 eV). The band gap (ΔE = LUMO-HOMO) is 3.20 eV for the sensor PTC (Fig. 7a). The deprotonation process of picric acid is favored when added to PTC in polar medium. This statement was previously

New Journal of Chemistry Accepted Manuscript

View Article Online
DOI: 10.1039/C9NJ02342A

Published on 10 June 2019. Downloaded by Nottingham Trent University on 6/22/2019 1:21:58 PM.

supported by ^{1}H NMR titration also. In fact, HOMO (-3.26 eV) of picrate situated above the LUMO of PTC-PA adduct (-3.73 eV) to favor the e^{-} migration process as shown in Fig. S20. However, HOMO energy level of the chemosensor resides below to the LUMO of PA (HOMO-LUMO gap is higher in PA in comparison to PTC; ΔE = 4.65 eV) causing the lower probability of GS charge transfer from chemosensor to PA. This phenomenon may be attributed to the static fluorescence quenching of fluorophore.[35] Similar kind of DFT mediated sensing mechanism has been also reported for anthracene and some other π-conjugated systems.[2, 3, 19]

Apart from that, in case of PTC-PA adduct, the HOMO (-6.35 eV) e^{-} density is located on the most e^{-} deficient picrate and that of LUMO (-3.73 eV) is occupied by sensor. Despite being stabilized in terms of HOMO as well as LUMO, PTC-PA adduct possesses lower band gap (ΔE = 2.62 eV) in compared to PTC. Therefore, the charge transfer process form HOMO to LUMO is preferred during the adduct formation between sensor and PA. As a result, considerable FL quenching was observed due to the decrement in ΔE value. The optical energy gaps (ΔE) of sensor and the corresponding adduct are calculated as per previous report, and are summarized in Table S6.

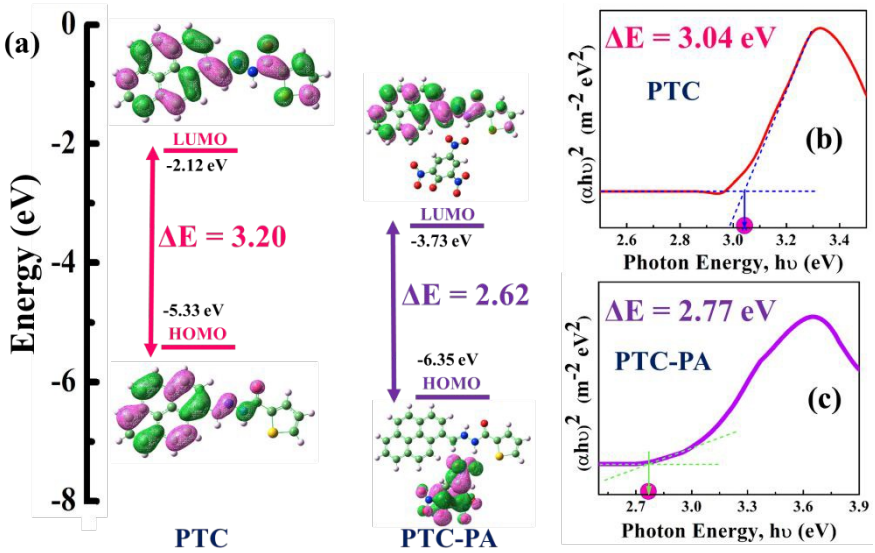

Fig. 7. (a) Pictorial representation of HOMO-LUMO molecular orbitals of chemosensor PTC and that of PTC-PA adduct, (b) and (c) compares the UV-Vis band gaps (ΔE) with those of theoretically calculated values.

As depicted in Fig. 7, the optical band gaps for the sensor and PTC-PA are 3.04 and 2.77 eV, respectively, which are in good agreement with those of theoretical values.

New Journal of Chemistry Accepted Manuscript

View Article Online
DOI: 10.1039/C9NJ02342A

Published on 19 June 2019. Downloaded by Nottingham Trent University on 6/22/2019 1:21:58 PM.

TDDFT calculations were performed to explain the UV-Vis and FTIR spectra. Fig. 8a-b shows a good correlation between the experimental and calculated absorbance and infrared spectra. Upon photon excitation, the donor to acceptor intramolecular charge transfer (ICT) is taking place to the extremely π-conjugated system of PTC. The ICT process prohibited when PTC is being coordinate to the Cu^{2+} ion, resulting in a sharp decrease in O.D. value at 368 nm. Spectral overlap theory can help to deeply understand the charge transfer process. Notably, the region covered by the absorption and emission spectral overlap of Cu-complex is very large with respect to PTC, leading to a preferable ICT process (Fig. 8c). In addition, as represented in Fig. 8d, the spectral overlap with the emission spectrum of sensor PTC is exceptionally low for PA in compared to picrate. Therefore, considerable spectral overlap can favor the energy transfer process from sensor to picrate, which could be another pathway for the FL quenching of PTC in solution phase.[21] In contrast, solid phase fluorescence quenching efficiency is quite small and less sensitive as PA to picrate conversion (deprotonation ability) in solid state during contact with sensor is very less.

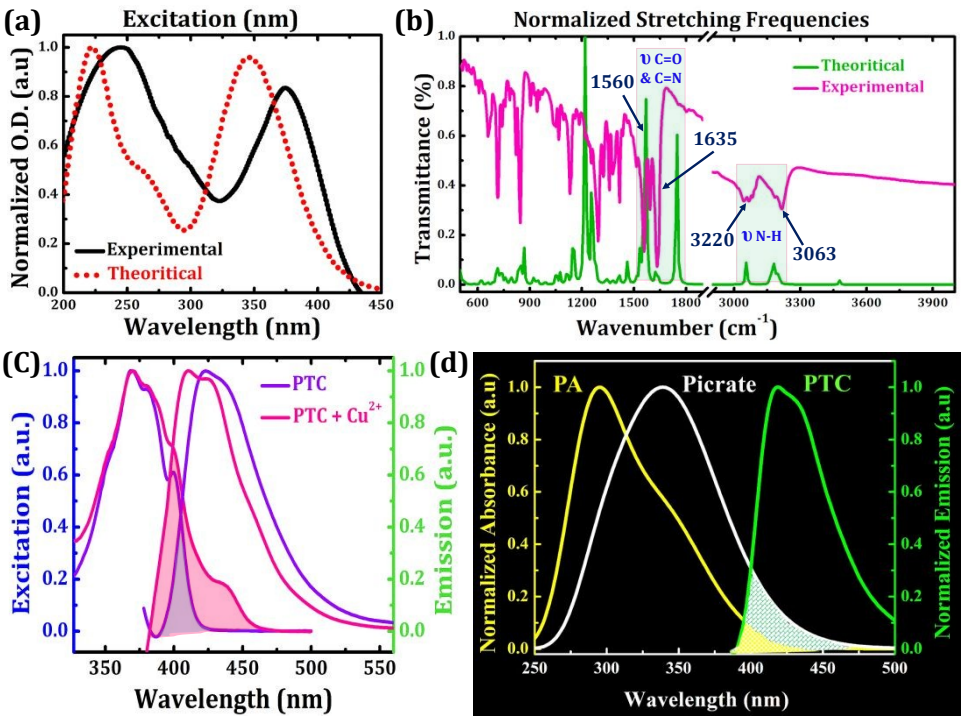

Fig. 8. (a) The experimental (black), and theoretical (red) normalized UV-visible spectra. (b) The calculated (pink) and experimental (green) stretching frequencies in FTIR spectrum. (c) Spectral overlap between absorption and emission spectra of PTC and its Cu-complex. (d) Spectral overlap between UV-visible spectra of PA and picrate with the emission spectra of sensor PTC.

New Journal of Chemistry Accepted Manuscript

View Article Online
DOI: 10.1039/C9NJ02342A

Published on 10 June 2019. Downloaded by Nottingham Trent University on 6/22/2019 1:21:58 PM.

New Journal of Chemistry Accepted Manuscript

Cell imaging study

Apart from the explosive sensing, fluorescence properties of the chemosensor PTC as well as PTC + Cu^{2+} adduct were used for confocal imaging. A549 cell lines were incubated with Cu^{2+} followed by treatment of PTC (10 µg/mL) for 1h at 37 °C. As depicted in Fig. 9, the control experiment with only Cu^{2+} ion never shows any imaging capabilities, whereas, that of PTC and PTC + Cu^{2+} complex can clearly discriminate the binding motif inside the cells.

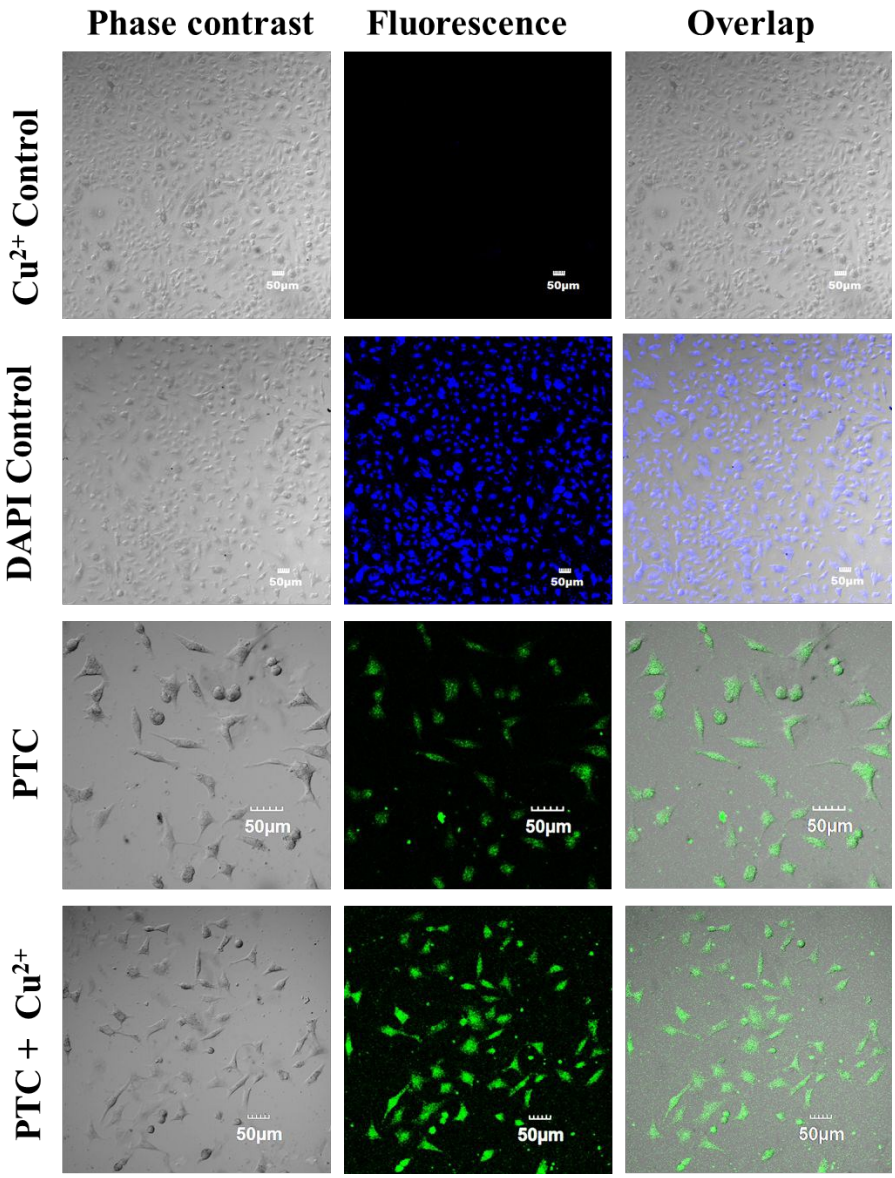

Fig. 9. Fluorescence images of A549 cancer cells with DAPI control (100 ng/mL), Cu^{2+}, PTC, and corresponding PTC + Cu^{2+} complex (10 µg/mL). Blue laser filter of wavelength 405 nm has been used during confocal microscopy.

DAPI has been used as a positive control in the similar emission range. Result shows that the intensity of fluorescence imaging enhances for PTC + Cu^{2+} complex with respect to blank

View Article Online
DOI: 10.1039/C9NJ02342A

PTC. Hence, PTC and PTC + Cu^{2+} complex possesses cell permeable nature, and can be used for the living cell imaging.

CONCLUSION

In conclusion, we have demonstrated a new pyrene based fluorescent chemosensor to detect Cu^{2+} and picric acid in CH_3CN and many other polar solvents. The probe has been found to be a potential candidate to act as copper(II) ion and nitro-explosive (PA) detector even by naked eyes. It is also suitable for environmental monitoring of those species and the efficacy of the probe has been found to be comparable to other existing NAC sensors (Table S7). Theoretical calculations strongly support the experimental results which includes spectroscopic reliability and, mechanistic pathways of explosive sensing. Additionally, PTC can also be useful to detect Cu^{2+} inside the living cells. Apart from that, the thermodynamical aspect, which is a key to understand about the reaction spontaneity of PTC-PA adduct, has been explored. More importantly, this is the first report of detailed temperature dependent thermodynamic investigation for picric acid sensing, which we have established in this literature.

ASSOCIATED CONTENT

Supporting Information.

This material is available free of charge via the Internet at http://pubs.acs.org. Synthetic procedures, instrumentation, and analytical characterization data. Fig. S1-S20† including ^{1}H, ^{13}C NMR, FTIR, UV-Vis, Fluorescence, Hand-held camera pictures for colorimetric detection, X-ray crystallography, DFT calculated energy gaps, sensing applications. Table S1-S7†. CCDC **1861748** is for PTC.

AUTHOR INFORMATION

Corresponding Author

*E-mail: suman@iiti.ac.in.

Author Contributions

The manuscript was written through contributions of all authors. All authors have given approval to the final version of the manuscript.

Funding Sources

Published on 10 June 2019. Downloaded by Nottingham Trent University on 6/22/2019 1:21:58 PM.

New Journal of Chemistry Accepted Manuscript

View Article Online
DOI: 10.1039/C9NJ02342A

This work is supported by DST India under Indo-Portuguese joint collaborative project scheme (Grant Number INT/PORTUGAL/P-04/2013).

Notes

The authors declare no competing financial interests.

ACKNOWLEDGMENT

Thankful to IIT Indore for the doctoral fellowships. The analytical supports received from SIC, IIT Indore, are gratefully acknowledged. Support by SERB, DST India (INT/PORTUGAL/P-04/2013) is gratefully acknowledged.

ABBREVIATIONS

NMR, nuclear magnetic resonance; ESI-MS, electrospray ionization mass spectrometry; PL/FL, photo-luminescence/ fluorescence; PET, photo-induced electron transfers; DFT, density functional theory.

REFERENCES

1. N. Ular, A. Üzer, S. Durmazel, E. Erçağ and R. Apak, *ACS Sensors*, 2018, 3, 2335-2342.
2. Z.-H. Fu, Y.-W. Wang and Y. Peng, *Chem. Commun.*, 2017, 53, 10524-10527.
3. K. Maiti, A. K. Mahapatra, A. Gangopadhyay, R. Maji, S. Mondal, S. S. Ali, S. Das, R. Sarkar, P. Datta and D. Mandal, *ACS Omega*, 2017, 2, 1583-1593.
4. S. Shanmugaraju and P. S. Mukherjee, *Chem. Commun.*, 2015, 51, 16014-16032.
5. M. Rong, L. Lin, X. Song, T. Zhao, Y. Zhong, J. Yan, Y. Wang and X. Chen, *Anal. Chem.*, 2015, 87, 1288-1296.
6. X. Sun, J. He, Y. Meng, L. Zhang, S. Zhang, X. Ma, S. Dey, J. Zhao and Y. Lei, *J. Mater. Chem. A*, 2016, 4, 4161-4171.
7. T.-P. Huynh, A. Wojnarowicz, A. Kelm, P. Woznicki, P. Borowicz, A. Majka, F. D'Souza and W. Kutner, *ACS Sensors*, 2016, 1, 636-639.
8. S. Mukherjee, A. V. Desai, A. I. Inamdar, B. Manna and S. K. Ghosh, *Cryst. Growth Des.*, 2015, 15, 3493-3497.
9. S. Huang, Q. He, S. Xu and L. Wang, *Anal. Chem.*, 2015, 87, 5451-5456.
10. B. Naskar, A. Bauzá, A. Frontera, D. K. Maiti, C. Das Mukhopadhyay and S. Goswami, *Dalton Trans.*, 2018, 47, 15907-15916.
11. S. Senapati and K. K. Nanda, *ACS Sustain. Chem. Eng.*, 2018, 6, 13719-13729.
12. K. Ponnuvel, G. Banuppriya and V. Padmini, *Sens. Actuators, B,* 2016, 234, 34-45.
13. S. Kumari, S. Joshi, T. C. Cordova-Sintjago, D. D. Pant and R. Sakhuja, *Sens. Actuators, B,* 2016, 229, 599-608.
14. T. Luo, Y. Li, Y. Xu, S. Zhang, Y. Wang, X. Kou and D. Xiao, *Sens. Actuators, B,* 2017, 253, 231-238.
15. A. F. Khasanov, D. S. Kopchuk, I. S. Kovalev, O. S. Taniya, K. Giri, P. A. Slepukhin, S. Santra, M. Rahman, A. Majee, V. N. Charushin and O. N. Chupakhin, *New J. Chem.*, 2017, 41, 2309-2320.
16. H. Lu, S. Quan and S. Xu, *J. Agric. Food. Chem.*, 2017, 65, 9807-9814.

Published on 10 June 2019. Downloaded by Nottingham Trent University on 6/22/2019 1:21:58 PM.

New Journal of Chemistry Accepted Manuscript

View Article Online
DOI: 10.1039/C9NJ02342A

Published on 10 June 2019. Downloaded by Nottingham Trent University on 6/22/2019 1:21:58 PM.

17. X. Qi, Y. Jin, N. Li, Z. Wang, K. Wang and Q. Zhang, *Chem. Commun.*, 2017, 53, 10318-10321.
18. S. Xu and H. Lu, *Chem. Commun.*, 2015, 51, 3200-3203.
19. A. H. Malik, S. Hussain, A. Kalita and P. K. Iyer, *ACS Appl. Mater. Interfaces*, 2015, 7, 26968-26976.
20. A. S. Tanwar, S. Hussain, A. H. Malik, M. A. Afroz and P. K. Iyer, *ACS Sensors*, 2016, 1, 1070-1077.
21. A. Chowdhury and P. S. Mukherjee, *J. Org. **Chem.***, 2015, 80, 4064-4075.
22. A. S. Tanwar, L. R. Adil, M. A. Afroz and P. K. Iyer, *ACS Sensors*, 2018, 3, 1451-1461.
23. P. Taya, B. Maiti, V. Kumar, P. De and S. Satapathi, *Sens. Actuators, B*, 2018, 255, 2628-2634.
24. A. K. Bar, S. Shanmugaraju, K.-W. Chi and P. S. Mukherjee, *Dalton Trans.*, 2011, 40, 2257-2267.
25. A. Senthamizhan, A. Celebioglu, S. Bayir, M. Gorur, E. Doganci, F. Yilmaz and T. Uyar, *ACS Appl. Mater. Interfaces*, 2015, 7, 21038-21046.
26. X. Wang, J. Bian, L. Xu, H. Wang and S. Feng, *Phys. Chem. Chem. Phys.*, 2015, 17, 32472-32478.
27. Y. Upadhyay, T. Anand, L. T. Babu, P. Paira, G. Crisponi, A. K. Sk, R. Kumar and S. K. Sahoo, *Dalton Trans.*, 2018, 47, 742-749.
28. J. Laborde, C. Deraeve, L. Lecoq, A. Sournia-Saquet, J.-L. Stigliani, B. S. Orena, G. Mori, G. Pratviel and V. Bernardes-Génisson, *ChemistrySelect*, 2016, 1, 172-179.
29. B. K. Kundu, R. Singh, R. Tiwari, D. Nayak and S. Mukhopadhyay, *New J. Chem.*, 2019, 43, 4867-4877.
30. B. K. Kundu, V. Chhabra, N. Malviya, R. Ganguly, G. S. Mishra and S. Mukhopadhyay, *Micropor. Mesopor. Mat.*, 2018, 271, 100-117.
31. B. K. Kundu, P. Mandal, B. G. Mukhopadhyay, R. Tiwari, D. Nayak, R. Ganguly and S. Mukhopadhyay, *Sens. Actuators, B*, 2019, 282, 347-358.
32. M. S. Mathew and K. Joseph, *ACS Sustain. Chem. Eng.*, 2017, 5, 4837-4845.
33. J. Keizer, *J. Am. Chem. Soc.*, 1983, 105, 1494-1498.
34. A. Saghatelian, N. H. Völcker, K. M. Guckian, V. S. Y. Lin and M. R. Ghadiri, *J. Am. Chem. Soc.*, 2003, 125, 346-347.
35. K. Acharyya and P. S. Mukherjee, *Chem. Commun.*, 2014, 50, 15788-15791.

New Journal of Chemistry Accepted Manuscript

View Article Online
DOI: 10.1039/C9NJ02342A

Mechanistic and thermodynamical aspects of pyrene based fluorescent probe to detect picric acid

Bidyut Kumar Kundu,[a] Pragti,[a] Reena,[a] Shaikh M. Mobin[a] and Suman Mukhopadhyay*[a,b]

[a]Discipline of Chemistry, School of Basic Sciences, Indian Institute of Technology Indore, Khandwa Road, Simrol, Indore 453552, India. Tel: +91 731 2438 735 Fax: +91 731 2361 482

[b]Discipline of Biosciences and Biomedical Engineering, School of Engineering, Indian Institute of Technology Indore, Khandwa Road, Simrol, Indore 453552, India.

*Contact E-mail: suman@iiti.ac.in; Fax: +91 731 2361; Tel: +91 731 2438 735

Graphical Abstract

Thermodynamical investigation of picric acid sensing by a pyrene based fluorescent probe.

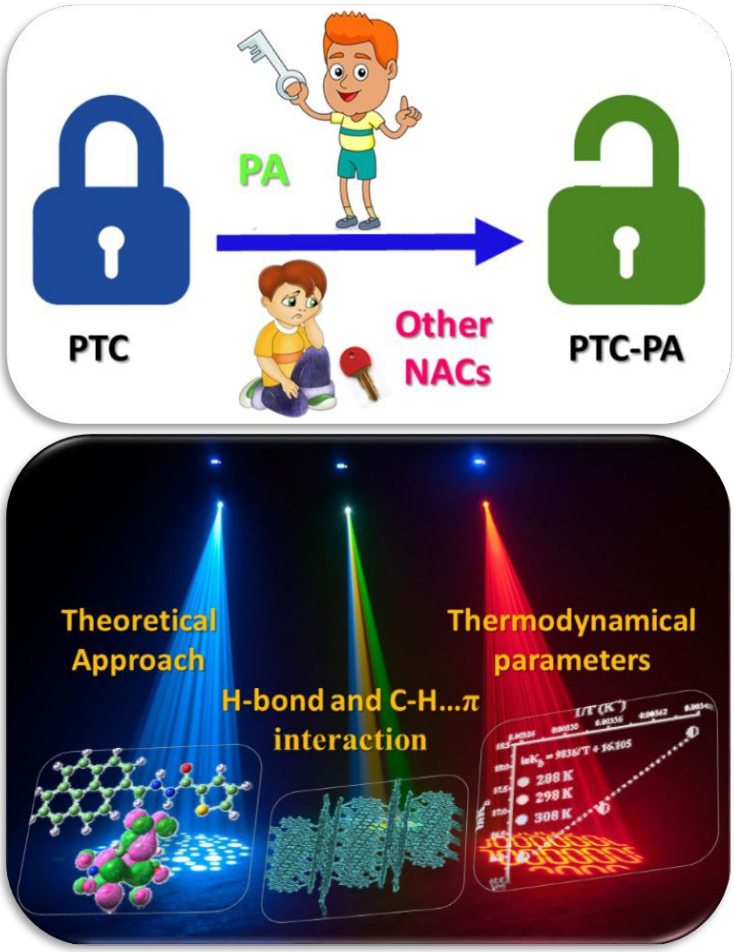

Published on 10 June 2019. Downloaded by Nottingham Trent University on 6/22/2019 1:21:58 PM.

New Journal of Chemistry Accepted Manuscript